ANNALS OF GEOPHYSICS, 65, 5, GT537, 2022; doi:10.4401/ag-8719
OPEN ACCESS

Exploring the Kinematic Structure of Mount Etna Volcano (Sicily, Italy) by Deformation Analysis and Gravity Gradient Tensors

Ayça Çırmık[*,1], Fikret Doğru[2], Oya Ankaya Pamukçu[1], Başak Turguz[1], Alessandro Bonforte[3]

(1) Dokuz Eylul University, Engineering Faculty, Department of Geophysical Engineering, Izmir, Turkiye
(2) Ataturk University, Oltu Vocational College, Construction, Erzurum, Turkiye
(3) Sezione di Catania, Istituto Nazionale di Geofisica e Vulcanologia, Piazza Roma 2, I-95123 Catania, Italy

Article history: received July 9, 2021; accepted July 26, 2022

Abstract

Ground deformation monitoring of active volcanoes is used routinely to determine phases of volcano unrest and can provide insights in the evolving plumbing system of a volcano and the influence local tectonics structures have on the volcano tectonic evolution of the volcanic edifice. Volcanic deformation analysis can be performed using velocity and direction measurements of the ground surface using Global Navigation Satellite System (GNSS). In this study, we perform two-dimensional deformation analyses of pre- and post-eruptive phases with the scope of determining the strain before and after an eruptive phase at Mt. Etna Volcano (southern Italy) during 2004-2006. In order to do so, we analyse the GNSS displacement data from Mt. Etna between 2004-2005 and 2005-2006 using the dedicated SSPX software. The extention, dilation and rotation maps of the study area were determined. The contraction and volumetric decrease concomitant the 2004-2005 effusive eruptive period and extension and volumetric increase for the 2005-2006 data series were observed. The deformation on the northeast part of Mt. Etna Volcano, which showed different characteristics with respect to its surroundings, was thought to be conditioned by the dynamic of the Pernicana fault system. Additionally, Complete Spherical Bouguer (CSB) gravity anomaly and the gravity gradient tensors were calculated giving insight on the subsurface structures of Mt. Etna Volcano and its surroundings.

Keywords: Mount Etna Volcano; GNSS; Deformation; Gravity; Gradient tensor

1. Introduction

Active volcanoes pose threat to human life and infrastructures. Volcanic hazards can be mitigated operating continuous detailed monitoring activity on individuate phases of volcano unrest with the aim of predicting the start of an eruption. To determine the volcanic activity types and their hazards, volcanoes are monitored with geophysical methods, such as geodetic, seismic, gravimetric and magnetic methods and thermal sensing studies [Rymer et al.,

1993; Budetta et al., 1999; Branca et al., 2003; Carbone et al., 2003; 2006; 2008; 2009]. GNSS measurements, if opportunely collected and processed, can provide three-dimensional position data with high accuracy, hence they are considered a suitable method for monitoring surface deformation of volcanoes, landslide, dams, etc. [Janssen, 2003]. Volcano deformation can be monitored and analyzed using velocity and direction information of selected benchmarks on the ground, obtained by GNSS measurements recorded in each time period.

To measure short-term deformation, the surveying frequency must be increased to follow ongoing phenomena. Therefore, forecast uncertainties in active volcanic zones can be overcome by adopting a deformation monitoring approach and implementing continuous GNSS measurements [Janssen, 2003].

GNSS measurements have been carried out on Mt. Etna since the late 1980s [Puglisi et al., 2001; Puglisi and Bonforte, 2004; Janssen, 2007; Larson et al., 2010 and the references therein], leading to the first models of the magmatic and structural framework of the volcano [Puglisi et al., 2001; Bonforte and Puglisi, 2003; 2006]. In this study, displacements measured during GNSS campaigns in 2004-2005 and 2005-2006 [Bonforte et al., 2008] of Mt. Etna volcano are analysed using the dedicated SSPX software [Cardozo and Allmendinger, 2009]. Considering that the volcano was active during the whole period covered by this study (2004 to 2006), the deformation of the volcano and its surroundings were interpreted as during and after the eruption and the deformation in the two data sets was compared. The selected two periods are very interesting for our purposes because they show an opposite behavior characterized by a syn-eruptive long-lasting deflation from 2004 to 2005, immediately followed by a renewal of magmatic recharging in the next year, from 2005 to 2006 [Bonforte et al., 2008]. Most of the investigations on Mt. Etna, over different time periods, evidenced a complex storage and feeding system coming from depth beneath the western side of the volcano, coupled with an outstanding dynamics affecting the eastern side of the edifice [e.g. Bonforte et al., 2011; Alparone et al., 2011 and 2013; Castro-Melgar et al., 2021]. In this study, we want to add some further information about the internal structure of the volcano, which is crucial for understanding the complex structural framework and dynamics affecting the volcano.

Additionally, as a second complementary analysis, the complete spherical Bouguer gravity anomaly of the World Gravity Model 2012 (WGM2012) model and the gravity gradient tensors (Txx, Txy, Txz, Tyy, Tyz and Tzz) were calculated. WGM 2012 model is the combination of the Earth Gravitational Model 2008 (EGM2008) [Pavlis et al., 2008] and the Global Ocean Tide Model DTU10 (Technical University of Denmark). In order to calculate the gravity tensors, the potential of the CSB gravity anomaly is computed and the second order derivatives of the potential anomaly are calculated along the x, y and z directions. It is observed that Mt. Etna has a lower CSB gravity anomaly and gravity gradient tensors (Tyy and Tzz) values than its surroundings.

Thus, we evaluate the gravity gradient tensors and compare them to the deformation analysis results and the kinematic structures of the studied region.

2. The Tectonic and Volcanic Activity of Mount (Mt.) Etna Volcano

Mount Etna is located in Eastern Sicily (souther Italy) and beside being the tallest basaltic-composite volcano (stratovolcano) in Europe [Romano, 1982; Bonaccorso et al., 2004; Behncke et al., 2008; Branca et al., 2008], rising more than 3300 m above sea level, is also among the most active volcanoes of the world. Mt. Etna Volcano dominates Catania, the second largest city of Sicily, and has one of the longest historical records of volcanism, thanks to the early ancient civilization of the area, starting from to 1500 BC. At Mt. Etna volcano, sometimes two types of eruptive activity can occur simultaneously. Permanent explosive eruptions occur from one or more summit craters, sometimes accompanied by minor lava emissions, often threatening villages and touristic infrastructures along the flanks of the volcano down to 1000 m asl. The volcano summit hosts 4 main active craters: the Bocca Nuova (BN), Voragine (VOR), Northeast Crater (NEC) and the complex of the Southeast Crater (SEC). After the 2004-2005 activities, a new crater formed on the eastern flank of the Southeast Crater, rapidly building a new cone over the old one, called The New South East crater (NSEC) [GVP, 2013; 2018; Acocella et al., 2016].

The structural architecture of the Mt. Etna area is mainly characterized by overall N-S compression and E-W extension along the Eastern Sicily coast and characterized by local complex tectonic arrangements [Bousquet and Lanzafame, 2004]. From the geodynamic point of view, Mt. Etna is located at the front of the Apennine-Maghrebian chain and at the intersection of the Malta Escarpment and Messina-Fiumefreddo structural line. The Malta Escarpment separates the oceanic Ionian basin from the continental African plate while the Messina-Fiumefreddo line represents the extensional zone along South Calabria and Northeast Sicily [Hirn et al., 1997; Azzaro 1999]. The

eastern side of the volcano is cut by several fault systems, related to this complex tectonic framework and to the local dynamics of this flank, continuously sliding towards the sea. The geodynamic character of Mt. Etna Volcano is in fact controlled by lateral instability processes [Urlaub et al., 2018]. Due to this situation, it has been observed that the eastern flank of the volcano moves towards the sea as a result of the complex interaction of regional tectonic stresses and the gravitational force acting on the volcanic edifice [Neri et al., 1991; Borgia et al., 1992; Lo Giudice and Rasa, 1992; McGuire et al., 1996; Rasa et al., 1996; Azzaro, 1999; Schiavone and Loddo, 2007; Alparone et al., 2011; Barreca et al., 2018a; b]. Geodetic studies from GNSS and InSAR measurements allowed the high-resolution mapping and characterization of the surface fault systems of Mt. Etna which can be grouped into different families, depending on their kinematic and role on the volcano flank dynamics (Bonforte et al., 2011; Azzaro et al., 2013; Barreca et al., 2013). According to the names attributed to the several fault systems in the GIS database proposed by Barreca et al. (2013), the NNW-SSE trending Timpe Fault System (TFS, given as S. Venerina Fault, Linera Fault and Acireale Fault in Fig.1) is located on the eastern side of the volcano; the E-W Pernicana Fault System (PFS) cuts the NE side; Trecastagni and other NW-SE trending faults (SFS, South Fault System) dissect the southern and southeastern flank of the volcano [Azzaro et al., 1998a; b; Azzaro et al., 2013; Barreca et al., 2013] (Figure 1). The Pernicana and Trecastagni faults [Bonforte and Puglisi, 2003; Bonforte et al., 2009] constitute the northern and the southern borders of the volcano-tectonic structure of Mt. Etna, besides, the moving part is bounded to the west by NE rift and S rift zones, even if a minor southwards motion has been evidenced on the southern flank, confined to the west by the Ragalna Fault System (RFS) (Figure 1) [Rust and Neri, 1996; Alparone et al., 2013; Azzaro et al., 2013; Bonforte et al., 2013, Barreca et al., 2018]. The PFS is the most active and extensively studied tectonic structure of the Mt. Etna region [Azzaro et al., 2001; Acocella and Neri, 2005; Bonforte et al., 2007a]. It is

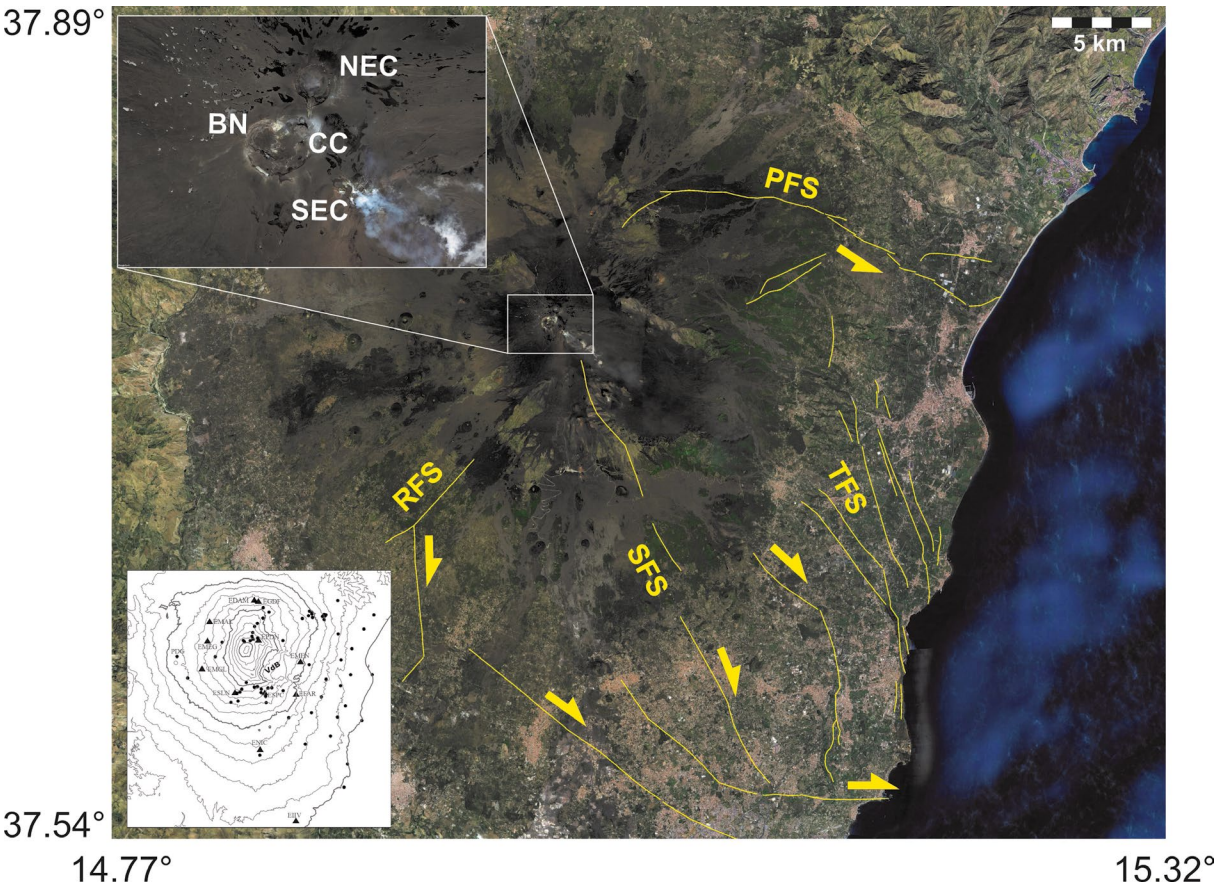

Figure 1. Mt. Etna satellite image with the main fault systems reported in the database in Barreca et al. [2013]. See text for the description and acronyms of the fault systems. The lower inset shows the GPS networks: Triangles for the permanent stations, dots for the periodic benchmarks. The upper inset shows a zoom on the summit craters: Bocca Nuova (BN); Central Crater (CC); North-East Crater (NEC); South-East Crater (SEC). Extent of the large area is the same as in Figure 2.

considered the northern boundary of the eastern flank of the volcano and it also accommodates and releases the stress induced by magmatic overpressure and/or intrusion events [Puglisi et al., 2001; Bonforte et al., 2007a; b; Alparone et al., 2011; 2013].

The western part of the volcano, which is more stable, responds to the deformation accumulated during the long-lasting inflation phases, indicating a permanent deformation of the volcano and therefore, permanent sub-surface magma storage in the volcano plumbing system.

3. GNSS Measurements at Mt. Etna

For volcano monitoring purposes, a permanent GNSS network with multiple receivers is established on selected and fixed geodetic monuments (benchmarks) on and around the volcano [see Bonforte et al., 2017 for a description of Mt. Etna geodetic networks and benchmarks for GNSS surveys]. Processing of the network data provides the positions of the benchmarks and then, by routinely repeating the measurements, the changes in the positions can be tracked through time, thus enabling the recognition of deformation anomalies [Aloisi et al., 2018]. The dense GNSS network on Mt. Etna is measured periodically (once per year, at least) and has more than seventy benchmarks. The time series of this network began in 1988 [Puglisi and Bonforte, 2004] and from then on, its configuration has been improved so that it now covers the entire volcanic area, with a particular emphasis on its eastern and north eastern flank. GNSS benchmarks are surveyed in static mode by carrying out sessions lasting from at least 4 hours to 24 hours. Eleven of these benchmarks are arranged in two small areas (about 1 square kilometer), across the Pernicana fault on its middle (RPN sub-network) and lower (RCN sub-network) sectors. Semi-kinematic occupations were used to survey 20 benchmarks aligned along a N-S profile reaching the summit area and along an E-W one on the middle southern flank of the volcano. The data collected during the surveys, combined with those coming from permanent stations, were processed using the National Geodetic Survey (NGS) antenna calibration models and precise ephemerides computed by the International Geodetic Service (IGS), adopting the usual procedure for the Etna network.

Ground deformation data are extremely important for following the evolution and movements of magma bodies beneath or within the volcano before they begin to fracture the hosting rocks, especially if coupled with other geophysical or geochemical evidence.

4. The SSPX Software for Deformation Analysis

Large-scale and high-resolution displacement and velocity data sets which can be obtainable by applying GNSS, radar interferometry, photogrammetry, digital image correlation and mechanical modelling techniques have been used by Earth scientists in recent years. Here we use the dedicated SSPX software to reconstruct the deformation during the period 2004-2006 using ground displacement and velocity data. The SSPX is a Macintosh, Cocoa/Universal application to calculate strain from displacement/velocity data in two and three dimensions [Cardozo and Allmendinger, 2009]. The SSPX calculates different types of deformation parameters (extension, shortening, dilatation and rotation) and provides the results as maps of their distribution over the investigated area [Cardozo and Allmendinger, 2009; Malaliçi, 2019; Malaliçi et al., 2019].

The displacement vector defines the position of the object with its origin or reference to the initial position. The displacement field is expressed as the assignment of displacement vectors for all points if the object is shifted from one position to another. The deformation can be defined as the change (gradient) of the displacement field as the most basic sense. Therefore, it is possible to calculate the deformation affecting the object by knowing the first and last positions of the object [Cardozo and Allmendinger, 2009].

5. Analysis

The surveys were carried out in 2004, 2005 and 2006 Bonforte et al. [2008] to detect ground deformation over the study area. Nevertheless, in this study a new and detailed re-analysis of those data has been performed in order to calculate the strain parameters and their spatial distribution and gradients. In this study, the displacement data obtained as a result of GNSS surveys [Bonforte et al., 2008] for the 2004-2005 and 2005-2006 periods on Mt. Etna volcano and its surroundings have been further analysed to calculate horizontal strain patterns and to be compared and integrated with gravity data. The data from 2004-2005 and 2005-2006 include the measurements from the July 2004 to July 2005 surveys and from the July 2005 to June 2006 surveys, respectively, integrated with the data acquired by the permanent Mt. Etna GPS network (Etn@net) during the surveys [Bruno et al., 2012]. The 2004 and 2005 measurements [Bonforte et al., 2008], were fixed to the reference frame, via the EIIV, CES and ROC coordinates outside and around the volcano edifice. For the 2005 measurements, a second adjustment process was done for obtaining an updated precise set of coordinates for the reference stations in the ITRF2000 frame, including NOT1, MATE, CAGL and LAMP IGS stations and their positions were fixed at the epoch 2005.6. The 2006 measurements were referred to the same reference frame as the 2005 measurements and the coordinates of MONT, ECES and EIIV were fixed with the second adjustment of the 2005 measurement [Bonforte et al., 2008]. During the observation period of the 2004-2005 measurements, an effusive eruption occurred from a fissure at the base of the SE crater. The effusive eruption followed a period of intense inflation and flank dynamics [Bonaccorso et al., 2006; Alparone et al., 2011] but started in September 2004 and continued until March 2005. During this eruption, the feeding system of the volcano has been emptied and the edifice was affected by a strong and wide deflation, due to the significant volume (ca. 60 millions of cubic meters, Fornaciai et al., 2021) of magma erupted. Conversely, between the 2005 and 2006 surveys, slight and sporadic activity was localized at the summit craters and the volcano's feeding system started to recharge, as confirmed by the general inflation observed by GPS measurements [Bonforte et al., 2008].

In this study, in order to determine the deformation before and after the eruption, the results of the deformation analyses were evaluated by taking into account that Mt. Etna volcano was erupting during the first year and recharging during the second. By using the SSPX software, the strain rate (Figures 2a, 2b), dilatation (Figures 3a, 3b) and rotation (Figures 4a, 4b) were calculated for the 2004-2005 and 2005-2006 GNSS displacement data [Bonforte et al., 2008].

Mt. Etna has a local gravity structure and gravity variations at various scales that are described in several papers [Rymer et al., 1993; Budetta et al., 1999; Branca et al., 2003; Carbone et al., 2003; 2006; 2008; 2009). For investigating the subsurface structures of Mt. Etna and its surrounding, the gravity anomalies and gravity gradient tensors were calculated. Therefore, as a satellite gravity model, the World Gravity Map 2012 (WGM2012) was selected and the complete spherical Bouguer (CSB) gravity anomaly was calculated (Figure 5) with the help of Bureau Gravimétrique International (BGI) service (http://bgi.omp.obs-mip.fr/data-products/Grids-and-models/wgm2012) [Bonvalot et al., 2012]. WGM2012 gravity anomalies were derived from the available Earth global gravity models; Earth Gravitational Model 2008 (EGM2008) [Pavlis et al., 2008] and Global Ocean Tide Model DTU10 (Technical University of Denmark) include 1'x1' resolution terrain corrections derived from ETOPO1 model at the global scale in spherical geometry. These models have been calculated utilizing a spherical harmonic approach using theoretical developments carried out to achieve accurate computations at a global scale [Balmino et al., 2011]. Afterwards, the potential of CSB anomaly was calculated in order to obtain the gravity gradient tensors (Txx, Txy, Txz, Tyy, Tyz and Tzz). Then, each tensor (Figure 6) were calculated as taking second-order derivatives along x, y and z directional using the Potensoft program [Arisoy and Dikmen, 2011] and besides, the high pass filter was applied for investigating the shallow structures (Figure 7). In this way, the boundaries of subsurface structures have become more visible. In addition, the interpretation of subtle structures has become more apparent by separating the anomalies of gravity tensors using a high pass filter.

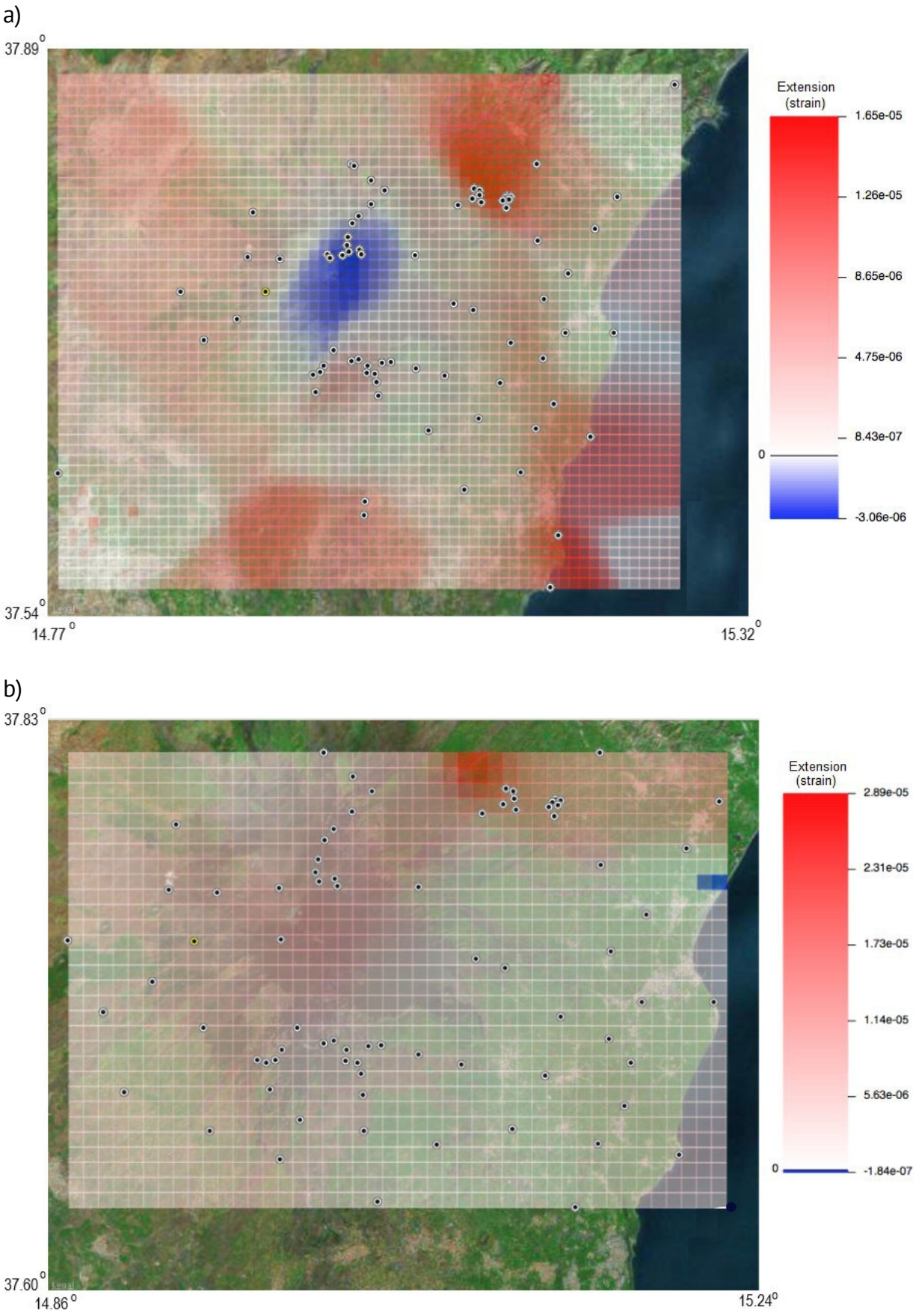

Figure 2. The strain rate pattern of Mt. Etna Volcano and its surroundings calculated from (a) 2004-2005 (b) 2005-2006 displacement data. Red and blue colours represent extension and contraction areas, respectively. The dots represent the locations of the GNSS stations.

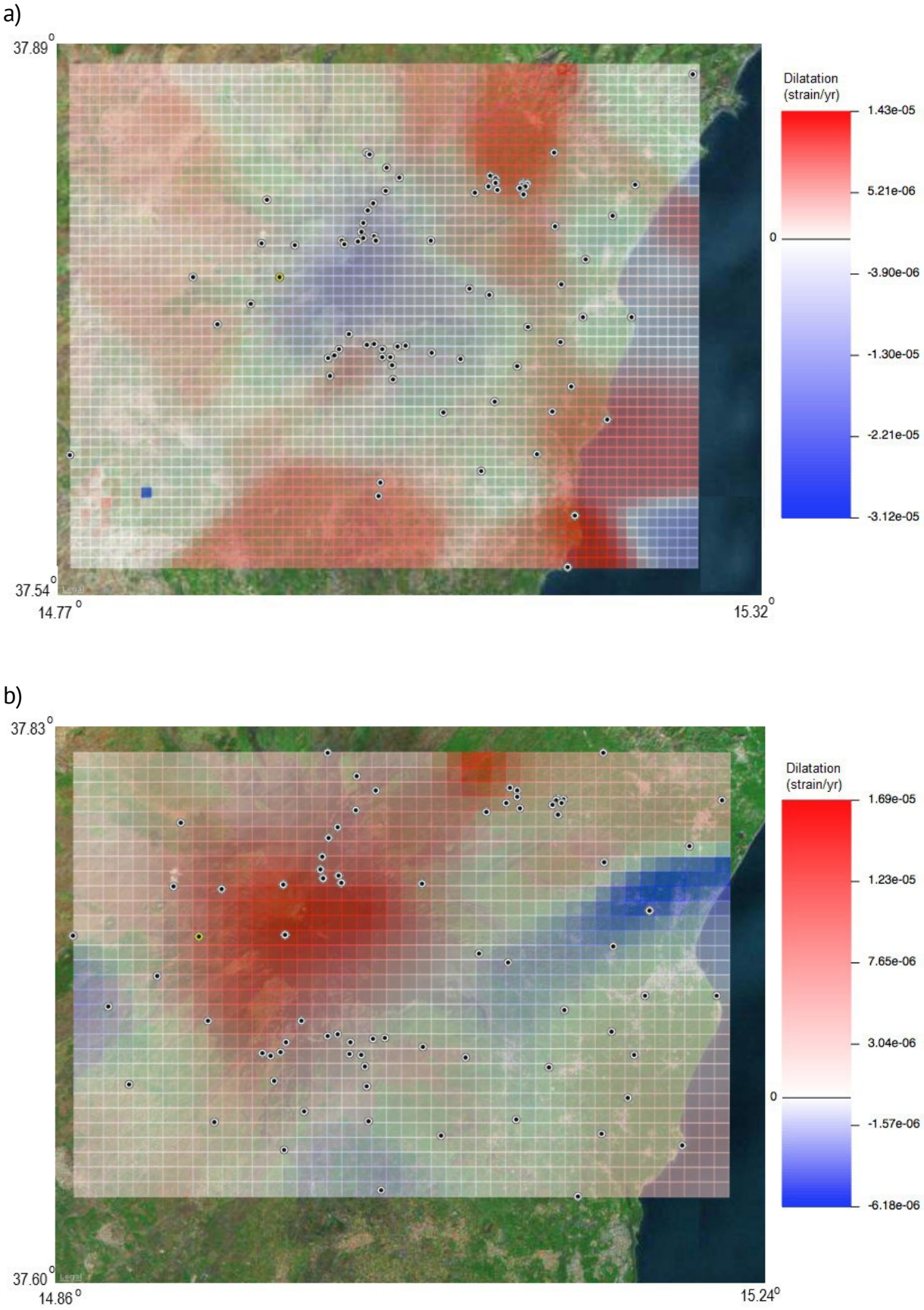

Figure 3. The dilatation maps of Mt. Etna Volcano and its surroundings calculated from (a) 2004-2005 (b) 2005-2006 displacement data. The dots represent the locations of the GNSS stations.

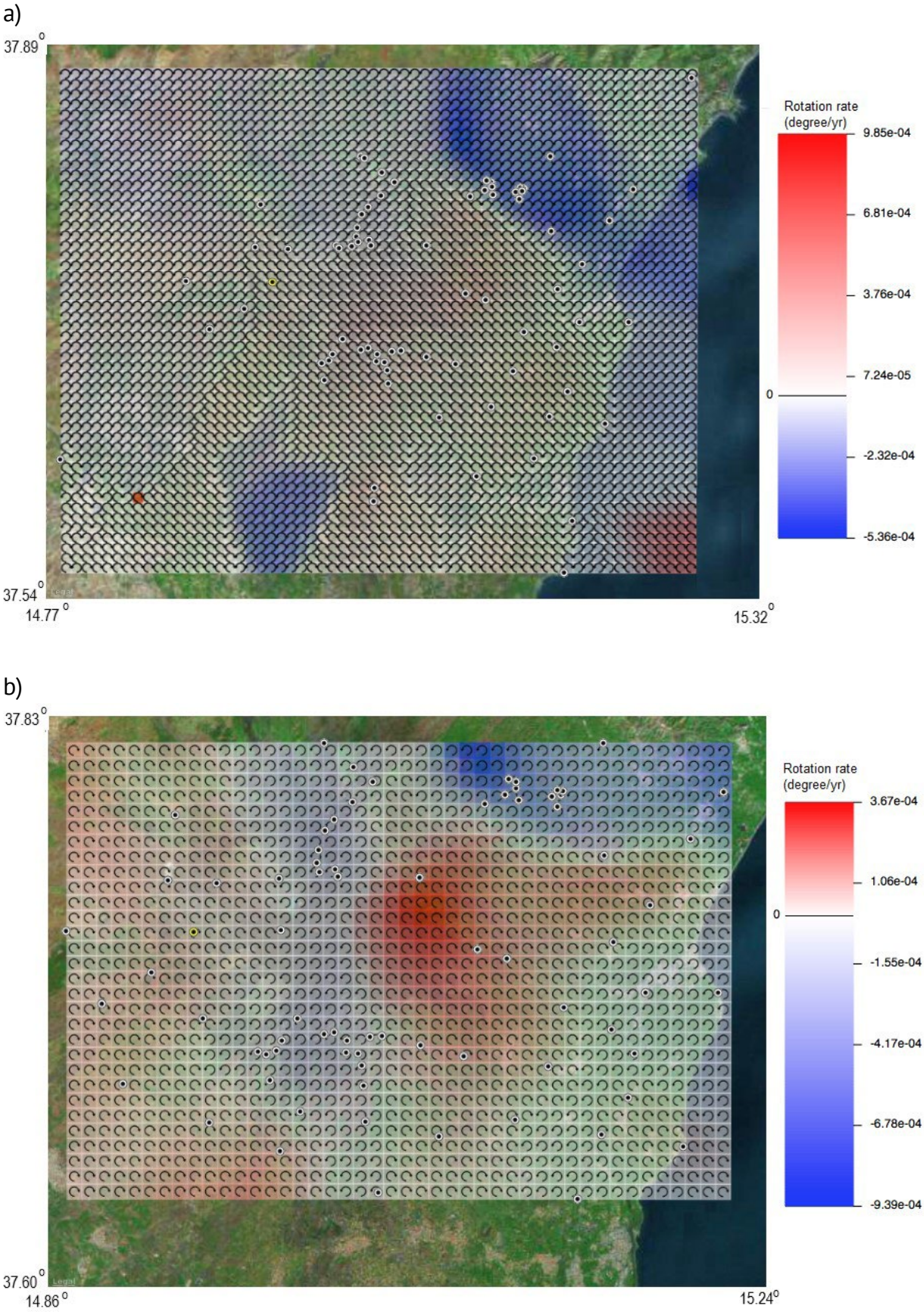

Figure 4. The rotation maps of Mt. Etna Volcano and its surroundings calculated from (a) 2004-2005 (b) 2005-2006 displacement data. Clockwise and counterclockwise represent positive and negative rotations, respectively. The dots represent the locations of the GNSS stations.

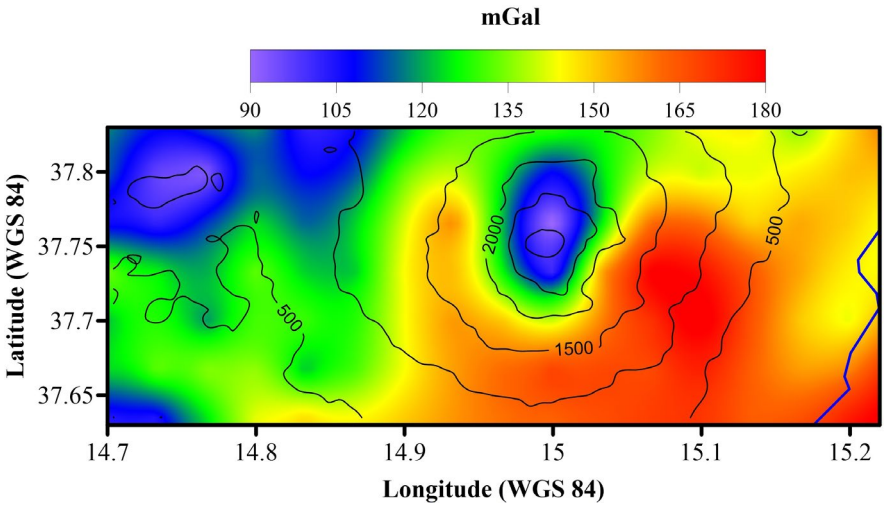

Figure 5. The complete spherical Bouguer (CSB) gravity anomaly of Mt. Etna and its surroundings with contoured on topography 500-meter grid spacing.

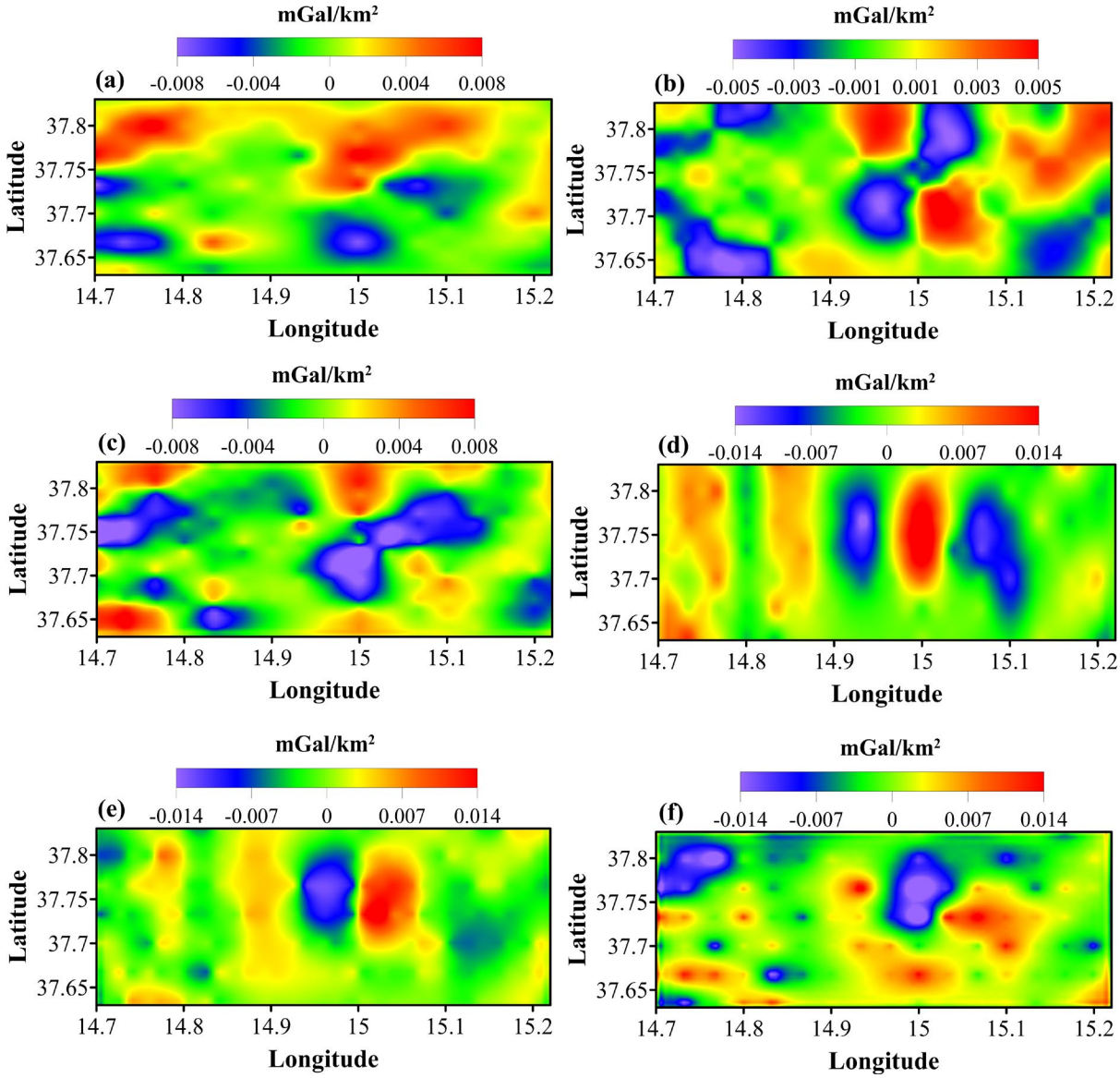

Figure 6. The gravity gradient tensors (a) Txx (b) Txy (c) Txz (d) Tyy (e) Tyz (f) Tzz.

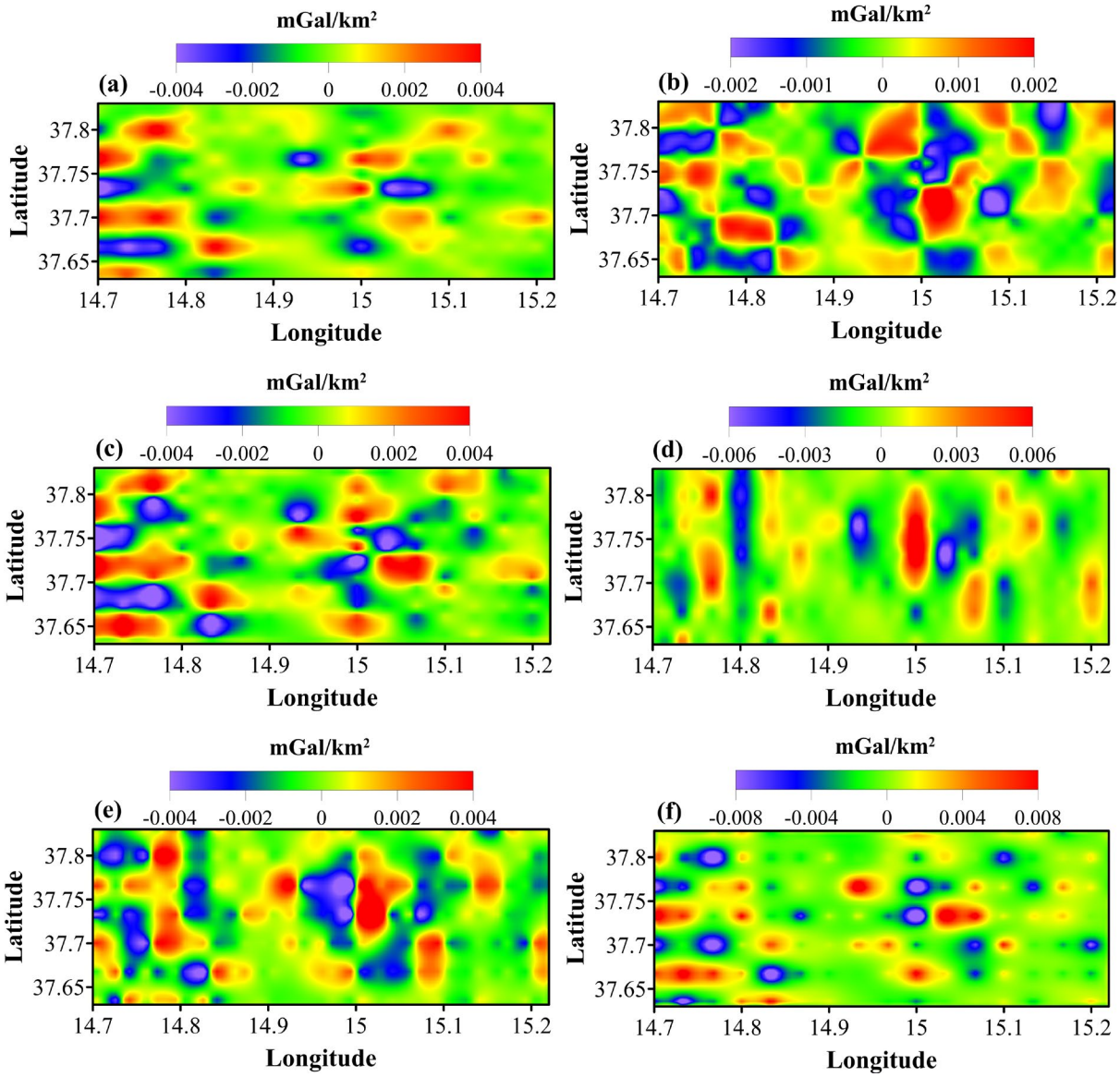

Figure 7. The high pass filter applied gravity gradient tensors (a) Txx (b) Txy (c) Txz (d) Tyy (e) Tyz (f) Tzz.

6. Results and Discussions

In this study, an analysis of the ground deformation pattern was performed for Mt. Etna Volcano, and the deformation patterns were contrasted with the gravity anomaly and gradient tensors of the region.

According to the strain rate during the 2004-2005 period (Figure 2a) (referred to as the "first period" in this section), extension is seen at NE side of the Mt. Etna Volcano while the contraction is seen on the summit part of the volcano. The extension during to the 2005-2006 interval (referred to as the "second period" in this section) (Figure 2b) is seen in the same region (NE side of the Mt. Etna Volcano) of the strain rate map of the first period (Figure 2a) and the amplitude of extension is similar during both measurement periods. Additionally, a contraction is noticed in the central part of the volcano for the first period (Figure 2a), an extension affects this area in the second period (Figure 2b). If the 2004-2005 eruption is considered, it can be confirmed that the contraction observed during the first period, related to the depletion of the feeding system, turned to extension (seen in the second period) after the end of the eruptive activity, indicating immediate recharging of the volcano. Meanwhile, the extension continued at the NE side during and after the activity.

In the dilatation map of the first period (Figure 3a), a high negative dilatation (decreasing in volume) is visible in the central region of the volcano and on its upper southwestern and south-eastern sides, while on the northeastern

side of Mt. Etna positive dilatation (increasing in volume) is seen. It appears that the positive and negative dilatation regions are coherent with the extension and contraction regions (Figure 2a). In the second period map (Figure 3b), while the positive dilatation affects the summit region, its NE side, negative dilatation is observed on three strips on the E, W and S flanks. Comparing both dilatation maps (Figures 3a and 3b), it can be said that the upper region of the volcano which shows negative dilatation in the first period (contraction) turns to positive dilatation and volumetric extend after the 2004-2005 activity.

In the rotation map of the first period (Figure 4a), while the NE side of the Mt. Etna Volcano shows a counterclockwise rotation north of the Pernicana fault, the central area, its Eastern and Southern sides present clockwise rotations. If the rotation map of the first period (Figure 4a) is compared with the strain rate (Figure 2a) and dilatation (Figure 3a) maps, it is seen that the NE side of Mt. Etna shows a different deformation relative to its surroundings. In the rotation map of the second period (Fig. 4b), the similar rotations with the first period (Figure 4a) are still seen at NE and Eastern Mt. Etna, while the direction of the rotation turns to counterclockwise on the summit region after the 2004-2005 activity. Therefore, it is thought that this different deformation is seen at NE of Mt. Etna could be caused by the effect of the dislocation along the Pernicana fault (Figure 1) where the ESE-wards movement of the eastern mobile flanks abruptly ends.

Comparing the Complete Spherical Bouguer (CBS) gravity map (Figure 5) and topograpyof Mt. Etna and its surroundings, it is seen that the central part of Mt. Etna, which has higher topography, shows lower gravity values. For this region, it is seen that the gravity anomalies are coherent with the topography, therefore, it can be said that there is an overall isostatic balance in this region [Watts, 2001; Pamukcu and Yurdakul, 2008; Pamukçu and Akçığ, 2011].

The knowledge about the movements and the properties of the tectonic structures is provided by evaluating the gravity and GNSS studies together [Çırmık, 2014; Çırmık et al., 2016; Çırmık and Pamukçu, 2017; Çırmık et al., 2017]. If the CSB gravity anomaly at Mt. Etna and its surroundings (Fig. 5) is evaluated with the vertical component (Up) values of 2004-2005 displacement data (Figure 8a), it is noticed that the changing pattern of vertical displacements and CSB anomalies are similar. Mt. Etna and its surroundings, centred at approximately 15° longitude and 37.75° latitude, represent relatively low gravity values, which is expected due to the possible high temperature shown in this region. Moreover, the vertical component (Up) values of the 2004-2005 displacement data (Figure 8a) turn negative at approximately 15° longitude and 37.75° latitude. The subsidence in the low-density hot regions causes decreased gravity values. Therefore, it is determined that the subsidence was more effective in the 2004-2005 period with respect to the 2005-2006 (Fig. 8a, b). In Fig. 8b, it is seen that the Up values of 2005-2006 displacement data are opposite with respect to the 2004-2005 data (Fig. 8a) at the summit and its surroundings. This means that the direction of the gravitational loading is upward and an uplift is seen in this region (Figure 8b). Accordingly, Bonforte et al. (2008) designated the 2004-2005 period as deflating phase and the 2005-2006 period as an inflating phase.

The gravity gradient tensors help to reveal the boundaries of the subsurface structures. With this perspective, if Tyy tensors of non-filtered (Fig. 6d) and high-pass filter applied (Figure 7d) gravity gradient tensors are examined, it can be observed that the subsurface lateral boundaries of Mt. Etna are better monitored in yy direction than other

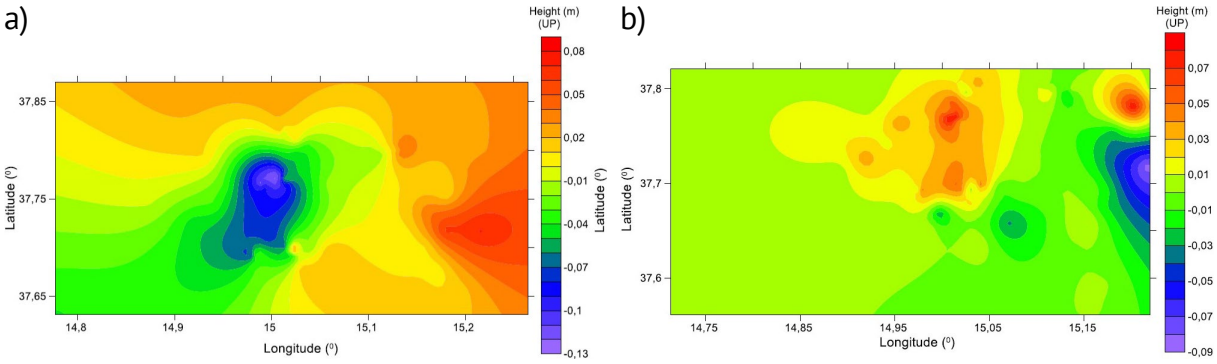

Figure 8. The vertical (Up) components of the displacement data (Bonforte et al., 2008) are relevant to (a) 2004-2005 and (b) 2005-2006 GNSS measurements.

directions. Besides, these subsurface horizontal boundaries are effective in a wider area than observed on the surface. This result shows that the extension of Mt. Etna in the W-E direction is more uniform.

In the gravity gradient tensors, it is known that Tzz represents the best coherency with the subsurface structures. Looking at the vertical (Up) components of the displacement data (Figure 8), it is noticed that the horizontal changes belonging to 2004-2005 data (Figure 8a) are coherent with the Tzz tensor (Figure 6f). Thus, the regions which show lower (subsidence areas) and higher depths (uplift areas) (Figure 8a) are consistent with the higher and lower gravity values (Fig. 6f), respectively. In the high-pass filtered tensor maps (Figure 7), the Tzz tensor (Figure 7f) represents two sources located under Mt. Etna. Bonaccorso et al. [2016] presented that there were double feeder sources in the Mt. Etna region, therefore, this hypothesis supports the result of Tzz tensor. If Tzz tensor of non-filtered gravity gradient tensors (Fig. 6f) and the strain rate map of 2004-2005 displacement data (Figure 2a) are evaluated together, it is seen that the anomalies are changing similarly at the summit and its surroundings. The vertical mass movement is effective in the strain rate of 2004-2005 displacement data (Fig. 2a). If the dilatation (Figure 4b) maps of 2005-2006 displacement data are compared with Tzz (Figure 7f), it is seen that vertical mass movement is effective in 2005-2006. Contrasting the deformation maps (Figures 2-4) created by SSPX using the displacement data with the gravity gradient tensors (Figures 6 and 7), it can be said that the vertical mass movement is more effective than the lateral mass movement in the regional mass deformation.

In its complex, the deformation analysis shows that the volcanic region of Mt. Etna represents compression and negative dilatation during the 2004-2005 eruption; after that activity, the region turns to an extension and positive dilatation. The northeastern side of the volcano presents higher amplitude and different deformation compared to its surroundings in all strain maps. Therefore, it is thought that this high amplitude deformation is not only related to the volcano activity, but also to the contribution of the active volcano-tectonic structures in the region.

References

Acocella, V. and M. Neri (2005). Structural features of an active strike-slip fault on the sliding flank of Mt. Etna (Italy), J. Struct. Geol., 27, 343-355.

Acocella, V., M. Neri, B. Behncke, A. Bonforte, C. Del Negro and G. Ganci (2016). Why does a mature volcano need new vents? The case of the New Southeast Crater at Etna. Frontiers in Earth Science, 4, 67.

Aloisi, M., A. Bonaccorso, F. Cannavò and G. Currenti (2018). Coupled Short- and Medium-Term Geophysical Signals at Etna Volcano: Using deformation and Strain to Infer Magmatic Processes from 2009 to 2017, Front. Earth. Sci., 6, 109.

Alparone, S., G. Barberi, A. Bonforte, V. Maiolino and A. Ursino (2011). Evidence of multiple strain fields beneath the eastern flank of Mt. Etna volcano (Sicily, Italy) deduced from seismic and geodetic data during 2003-2004, Bull. Volcanol., 73, 869-885, https://doi.org/10.1007/s00445-011-0456-1.

Alparone, S., A. Bonaccorso, A. Bonforte and G. Currenti (2013). Long-term stress-strain analysis of volcano flank instability: The eastern sector of Etna from 1980 to 2012, J. Geophys. Res. Solid Earth, 118, 5098-5108, doi:10.1002/jgrb.50364.

Arisoy, M. Ö. and Ü. Dikmen (2011). Potensoft: MATLAB-based software for potential field data processing, modeling and mapping, Compu. Geosci., 37, 7, 935-942.

Azzaro, R., L. Ferreli, A. L. Michetti, L. Serva and E. Vittori (1998a). Environmental hazard of capable faults: the case of the Pernicana fault (Mt. Etna, Sicily), Nat. Haz., 17, 147-162.

Azzaro, R., S. Branca, S. Giammanco, S. Gurrieri, R. Rasa and M. Valenza (1998b). New evidence for the form and extent of the Pernicana Fault System (Mount Etna) from structural and soil-gas surveying, J. Volcanol. Geotherm. Res., 84, 143-152.

Azzaro, R. (1999). Earthquake surface faulting at mount etna volcano (sicily) and implications for active tectonics, J. Geodynamics, 28, 193-213.

Azzaro, R., M. Mattia and G. Puglisi (2001). Fault creep and kinematics of the eastern segment of the Pernicana Fault (Mt. Etna, Italy) derived from geodetic observations and their tectonic significance, Tectonophysics, 333, 401-415.

Azzaro, R., A. Bonforte, S. Branca and F. Guglielmino (2013). Geometry and kinematics of the fault systems controlling the unstable flank of Etna volcano (Sicily), J. Volcanol. Geotherm. Res., 251, 5-15.

Balmino, G., N. Vales, S. Bonvalot and A. Briais (2011). Spherical harmonic modeling to ultra-high degree of Bouguer and isostatic anomalies, J. Geodesy, 86, 7, 499-520.

Barreca, G., A. Bonforte and M. Neri (2013). A pilot GIS database of active faults of Mt. Etna (Sicily): A tool for integrated hazard evaluation, J. Volcanol. Geotherm. Res., 251, 170-186.

Barreca, G., S. Branca and C. Monaco (2018a). Three-dimensional modeling of Mount Etna volcano: Volume assessment, trend of eruption rates, and geodynamic significance, Tectonics, 37, https://doi.org/10.1002/2017TC004851.

Barreca, G., M. Corradino, C. Monaco and F. Pepe (2018b). Active tectonics along the south east offshore margin of Mt. Etna: new insights from high-resolution seismic profiles, Geosci., 8, 2, 62.

Behncke, B., S. Calvari, S. Giammanco et al. (2008) Pyroclastic density currents resulting from the interaction of basaltic magma with hydrothermally altered rock: an example from the 2006 summit eruptions of Mount Etna, Italy, Bull. Volcanol., 70, 1249-1268. https://doi.org/10.1007/s00445-008-0200-7.

Bonaccorso, A., S. Calvari, M. Coltelli, C. Del Negro and S. Falsaperla (2004). Mt. Etna: Volcano Laboratory, 2004. AGU Monography 143. https://doi.org/10.1029/143GM14. Haraldur Sigurdsson (Editor). The Encyclopedia of Volcanoes (Second Edition), Academic Press, 2015, ISBN 9780123859389.

Bonaccorso, A., A. Bonforte, F. Guglielmino, M. Palano and G. Puglisi (2006). Composite ground deformation pattern forerunning the 2004-2005 Mount Etna eruption, J. Geophys. Res.: Solid Earth, 111, B12.

Bonaccorso, A., S. Calvari and E. Boschi (2016). Hazard mitigation and crisis management during major flank eruptions at Etna volcano: reporting on real experience, Geol. Soc., London, Special Pub., 426, 1, 447-461.

Bonforte, A. and G. Puglisi (2003). Magma uprising and flank dynamics on Mount Etna volcano, studied using GPS data (1994-1995), J. Geophys. Res., 108, https://doi.org/10.1029/2002JB001845.

Bonforte, A. and G. Puglisi (2006). Dynamics of the eastern flank of Mt. Etna volcano (Italy) investigated by a dense GPS network. J. Volcanol. Geotherm. Res., 153, 357-369, https://doi.org/10.1016/j.jvolgeores.2005.12.005.

Bonforte, A., S. Branca and M. Palano (2007a). Geometric and kinematic variations along the active Pernicana fault: implication for the Dynamics of Mount Etna NE flank (Italy), J. Volcanol. Geotherm. Res., 160, 210-222, doi:10.1016/ j.jvolgeores. 2006.08.00.

Bonforte, A., D. Carbone, F. Greco and M. Palano (2007b). Intrusive mechanism of the 2002 NE-rift eruption at Mt Etna (Italy) modelled using GPS and Gravity data, Geophys. J. Int., 169, 339-347, doi: 10.1111/j.1365-246X.2006.03249.x.

Bonforte, A., A. Bonaccorso, F. Guglielmino, M. Palano and G. Puglisi (2008). Feeding system and magma storage beneath Mt. Etna as revealed by recent inflation/deflation cycles, J. Geophys. Res., 1-13, B05406, doi: 10.1029/2007JB005334.

Bonforte, A., S. Gambino and M. Neri (2009). Intrusion of eccentric dikes: The case of the 2001 eruption and its role in the dynamics of Mt. Etna volcano, Tectonophys., 471, 78-86.

Bonforte, A., F. Guglielmino, M. Coltelli, A. Ferretti and G. Puglisi (2011). Structural assessment of Mount Etna volcano from Permanent Scatterers analysis, Geochemistry, Geophysics, Geosystems, 12(2), 1-19.

Bonforte, A., A. Carnazzo, S. Gambino, F. Guglielmino, F. Obrizzo and G. Puglisi (2013). A multidisciplinary study of an active fault crossing urban areas: The Trecastagni Fault at Mt. Etna (Italy), J. Volcanol. Geotherm. Res., 251, 41-49.

Bonforte, A., F. Guglielmino and G. Puglisi (2017). 2014-2016 Mt. Etna Ground deformation imaged by SISTEM approach using GPS and SENTINEL-1A/1B TOPSAR data, EGUGA, 13611.

Bonvalot, S., G. Balmino, A. Briais, M. Kuhn, A. Peyrefitte, N. Vales, R. Biancale, G. Gabalda, F. Reinquin and M. Sarrailh (2012). World Gravity Map. Commission for the Geological Map of the World. Eds. BGI-CGMW-CNES-IRD, Paris.

Borgia, A., L. Ferrari and G. Pasquare (1992). Importance of gravitational spreading in the tectonic evolution of Mount Etna, Nature, 357, 231-236.

Bousquet, J. C. and G. Lanzafame (2004). The tectonics and geodynamics of Mt. Etna: Synthesis and interpretation of geological and geophysical data, in Etna Volcano Laboratory, Geophys. Monogr. Ser., 143, edited by A. Bonaccorso et al., 29-47, AGU, Washington, D. C.

Branca, S., M. Coltelli, E. De Beni and J. Wijbrans (2008). Geological evolution of Mount Etna volcano (Italy) from earliest products until the first central volcanism (between 500 and 100 ka ago) inferred from geochronological and stratigraphic data, Int. J. Earth Sci., 97, 135-152, doi:10.1007/s00531-006-0152-0.

Branca, S., D. Carbone and F. Greco (2003). Intrusive mechanism of the 2002 NE-Rift eruption at Mt. Etna (Italy) inferred through continuous microgravity data and volcanological evidences, Geophys. Res. Lett., 30, 20, 2077.

Bruno, V., M. Mattia, M. Aloisi, M. Palano, F. Cannavò and W. E. Holt (2012). Ground deformations and volcanic processes as imaged by CGPS data at Mt. Etna (Italy) between 2003 and 2008, J. Geophys. Res., 117, B07208, doi:10.1029/2011JB009114.

Budetta, G., D. Carbone and F. Greco (1999). Subsurface mass redistributions at Mount Etna (Italy) during the 1995-1996 explosive activity detected by microgravity studies, Geophy. J. Int., 138, 1, 77-88.

Carbone, D., G. Budetta, F. Greco and H. Rymer, (2003). Combined discrete and continuous gravity observations at Mount Etna, J. Volcanol. Geotherm. Res., 123, 1-2, 123-135.

Carbone, D., L. Zuccarello, G. Saccorotti and F. Greco (2006). Analysis of simultaneous gravity and tremor anomalies observed during the 2002-2003 Etna eruption, Earth Planet. Sci. Lett., 245, 3-4, 616-629.

Carbone, D., L. Zuccarello and G. Saccorotti (2008). Geophysical indications of magma uprising at Mt Etna during the December 2005 to January 2006 non-eruptive period, Geophys. Res. Lett., 35(6), L06305

Carbone, D., P. Jousset and C. Musumeci (2009). Gravity "steps'' at Mt. Etna volcano (Italy): Instrumental effects or evidences of earthquake-triggered magma density changes, Geophys. Res. Lett., 36, L02301.

Cardozo, N. and R.W. Allmendinger (2009). SSPX: A program to compute strain from displacement/velocity data, Comp. Geosci., 35, 1343-1357.

Castro-Melgar, I., J. Prudencio, E. Del Pezzo, E. Giampiccolo and J. M. Ibanez (2021). Shallow magma storage beneath Mt. Etna: Evidence from new attenuation tomography and existing velocity models, Journal of Geophysical Research: Solid Earth, 126, 7, e2021JB022094.

Çırmık, A. (2014). Determining the deformation in Western Anatolia with GPS and gravity measurements, PhD. Thesis, Dokuz Eylul University, The Graduate School of Natural and Applied Sciences, Izmir, Turkey.

Çırmık, A., O. Pamukçu and Z. Akçığ (2016). Mass and stress changes in the Menderes Massif (western Anatolia, Turkey), J. Asian Earth Sci., 131, 109-122.

Çırmık, A., F. Doğru, T. Gönenç and O. Pamukçu (2017). The stress/strain analysis of kinematic structure at Gülbahçe Fault and Uzunkuyu Intrusive (Izmir, Turkey), Pure App. Geophy., 174, 3, 1425-1440.

Çırmık, A. and O. Pamukçu (2017). Clarifying the interplate main tectonic elements of Western Anatolia, Turkey by using GNSS velocities and Bouguer gravity anomalies, J.Asian Earth Sci., 148, 294-304.

DTU Space, National Space Instutute (Denmark). Global Mean SeaSurface. ftp.space.dtu.dk/pub/DTU10.

Fornaciai, A., D. Andronico, M. Favalli, L. Spampinato, S. Branca, L. Lodato, A. Bonforte and L. Nannipieri (2021). The 2004-2005 Mt. Etna compound lava flow field: a retrospective analysis by combining remote and field methods, J. Geophys. Res.: Solid Earth, 126, 3, e2020JB020499.

Global Volcanism Program (GVP) (2013). Volcanoes of the World, v. 4.9.1 (17 Sep 2020). Venzke, E (ed.). Smithsonian Institution, Downloaded 12 Oct 2020. https://doi.org/10.5479/si.GVP.VOTW4-2013.

Global Volcanism Program (GVP) (2018). Report on Etna (Italy) (Crafford, A.E., and Venzke, E., eds.). Bulletin of the Global Volcanism Network, 43, 12. Smithsonian Institution.

Hirn, A., R. Nicolich, J. Gallart, M. Laigle, L. Cernobori and the ETNASEIS Scientific Group. (1997). Roots of Etna volcano in faults of great earthquakes, Earth Planet Sci., 148, 7-9.

Janssen,V. (2003). A mixed-mode GPS network processing approach for volcano deformation monitoring. PhD. Thesis, University of New South Wales Sydney. Australia.

Janssen, V. (2007). Volcano deformation monitoring using GPS, J. Spatial Sci., 52, 1, 41-54.

Larson, K. M., M. Poland and A. Miklius (2010). Volcano monitoring using GPS: Developing data analysis strategies based on the June 2007 Kīlauea Volcano intrusion and eruption, J. Geophys. Res., 115, B07406, doi:10.1029/2009JB007022.

Lo Giudice and E. R. Rasa (1992). Very shallow earthquakes and brittle deformation in active volcanic areas: the Etnean region as example, Tectonophysics, 202, 257-268.

Malaliçi, B. C. (2019). Gülbahçe fayı ve çevresinin jeodinamik yapısının irdelenmesi, Msc Thesis, Dokuz Eylul University, The Graduate School of Natural and Applied Sciences, Izmir, Turkey, 77 (In Turkish).

Malaliçi, B. C., O. Pamukçu, A. Çırmık and H. Dindar (2019). Deformation Analysis of Cyprus and its surroundings (East Mediterranean) with using SSPX software, Dokuz Eylul University Faculty of Engineering Journal of Science and Engineering, 21, 61, 235-246.

McGuire, W. J., J. L. Moss, S. J. Saunders and I. S. Stewart (1996). Dyke-induced rifting and edifice instability at Mount Etna. In: Gravestock, P J and McGuire W J (Eds), Etna: fifteen years on, Cheltenham and Gloucester Special Publication.

Neri, M., V. H. Garduno, G. Pasquare and R. Rasa (1991). Studio strutturale e modello cinematico della Valle del Bove e del settore nord-orientale etneo, Acta Vulcanol., 1, 17-24.

Pamukcu, O. and A. Yurdakul (2008). Isostatic compensation in western Anatolia with estimate of the effective elastic thickness, Turkish J. Earth Sci., 17, 3, 545-557.

Pamukçu, O. A. and Z. Akçığ (2011). Isostasy of the Eastern Anatolia (Turkey) and discontinuities of its crust, Pure App. Geophy., 168, 5, 901-917.

Pavlis, N. K., S. A. Holmes, S. C. Kenyon and J. K. Factor (2008). An earth gravitational model to degree 2160: EGM2008, EGU general assembly, 10, 13-18.

Puglisi, G., A. Bonforte and S. R. Maugeri (2001). Ground deformation patterns on Mount Etna, 1992 to 1994, inferred from GPS data, Bull. Volcanol., 62, 371-384.

Puglisi, G. and A. Bonforte (2004). Dynamics of Mount Etna Volcano inferred from static and kinematic GPS measurements, J. Geophy. Res.: Solid Earth, 109, B11.

Rasa, R., R. Azzaro and O. Leonardi (1996). Aseismic creep on faults and flank instability at Mt. Etna volcano, Sicily. In: McGuire W C, Jones A P and Neuberg J. (Eds), Volcano Instability on the Earth and Other Planets, Geol. Soc. Special Pub., 110, 179-192.

Rymer, H., J. B. Murray, G. C. Brown, F. Ferrucci and W. J. McGuire (1993). Mechanisms of magma eruption and emplacement at Mt Etna between 1989 and 1992, Nature, 361, 6411, 439-441.

Romano, R. (1982). Succession of volcanic activity in the Etnean area, in Mount Etna Volcano a Review of Recent Earth Sciences Studies, Memorie della Società Geologica Italiana, 23, edited by R. Romano, 27-48, Bardi Editor, Rome, Italy.

Rust, D. and M. Neri (1996). The boundaries of large-scale collapse on the flanks of Mount Etna, Sicily. In: McGuire, W C, Jones A P and Neuberg J. (Eds), Volcano Instability on the Earth and Other Planets, Geol. Soc. Special Pub., 110, 193-208.

Schiavone, D. and M. Loddo (2007). 3-D density model of Mt. Etna Volcano (Southern Italy), J. Volcanol. Geotherm. Res, 164, 161-175.

Urlaub, M., F. Petersen, F. Gross, A. Bonforte, G. Puglisi, F. Guglielmino, et al. (2018). Gravitational collapse of Mount Etna's southeastern flank, Science Advances, 4 10.

Watts, A. B. (2001). Isostasy and Flexure of the Lithosphere. Cambridge University Press.

***CORRESPONDING AUTHOR: Ayça ÇIRMIK**,
Dokuz Eylul University, Engineering Faculty, Department of Geophysical Engineering, Izmir, turkey,
e-mail: ayca.cirmik@deu.edu.tr